Threshold effect with stochastic fluctuation in bacteria-colony-like proliferation dynamics as analyzed through a comparative study of reaction-diffusion equations and cellular automata

Kenta Odagiri and Kazuo Takatsuka
Department of Basic Science, Graduate School of Arts and Sciences, The University of Tokyo, 153-8902 Tokyo, Japan
(Received 9 April 2008; revised manuscript received 7 September 2008; published 2 February 2009)

We report a comparative study on pattern formation between the methods of cellular automata (CA) and reaction-diffusion equations (RD) applying to a morphology of bacterial colony formation. To do so, we began the study with setting an extremely simple model, which was designed to realize autocatalytic proliferation of bacteria (denoted as X) fed with nutrition (N) and their inactive state (prespore state) P_1 due to starvation: $X+N\rightarrow 2X$ and $X\rightarrow P_1$, respectively. It was found numerically that while the CA could successfully generate rich patterns ranging from the circular fat structure to the viscous-finger-like complicated one, the naive RD reproduced only the circular pattern but failed to give a finger structure. Augmenting the RD equations by adding two physical factors, (i) a threshold effect in the dynamics of $X+N\rightarrow 2X$ (breaking the continuity limit of RD) and (ii) internal noise with onset threshold (breaking the inherent symmetry of RD), we have found that the viscous-finger-like realistic patterns are indeed recovered by thus modified RD. This highlights the important difference between CA and RD, and at the same time, clarifies the necessary factors for the complicated patterns to emerge in such a surprisingly simple model system.

DOI: 10.1103/PhysRevE.79.026202 PACS number(s): 89.75.Kd, 87.18.Hf, 82.40.Ck, 05.40.−a

I. INTRODUCTION

Nonlinear growth in multiple agent systems such as those in autocatalytic reactions is often associated with pattern formation ubiquitously, ranging from the atomic scale phenomena [1] to the morphology of living bodies [2]. It is quite interesting to explore how those diverse patterns are generally ruled, and indeed a large amount of literature has already been devoted to the related subjects [3–8].

Theoretical studies on nonlinear growth usually consist of two stages: (1) model setting, in which the mechanism of relevant dynamics is assumed and dominating components and physical factors are specified. It is quite often that the mechanism is represented in terms of a network of key reactions (actions), with the Oregonator model [9] for the Belousov-Zhabotinskii reaction being an illuminating example. (2) Numerical realization or simulations as a test of the assumed model and/or further analyses. The methods of reaction-diffusion equations (RD) and the cellular automaton (CA) are among the most widely used techniques. It is generally anticipated that theoretical results should not depend much on the choice of the method of simulation, aside from numerical efficiency, since they are designed to realize the model as faithfully as possible. However, to the best of our knowledge, there are few studies to examine whether this is really the case.

The aim of the present paper is twofold. We first survey an extremely simple autocatalytic proliferation model, Eqs. (1a) and (1b) for the growth of bacterial colony patterns [10–13] by means of CA, scanning the morphological diagram of *Bacillus subtilis* created by Matsushita *et al.* [10], which exhibits five different patterns depending on two experimental parameters: the initial nutritive concentration and the substrate softness (the mobility of bacterium). Furthermore, using this model, we compare RD and CA placing a focus on the formation of the viscous-finger-like pattern of the colony. In so doing, we identify a qualitative difference between RD and CA. Moreover, it turns out that the difference manifests the important physical factors that bring about the characteristic patterns of the bacterial colony.

Many studies of pattern formation made so far have used RD, which are often based on a mean-field description such as rate equations in chemical reaction systems. The greatest advantage of this method is that mathematical techniques to analyze the pattern formation and associated phenomena, such as the linear stability analysis around the fixed points, follow automatically. These analytical techniques are very powerful indeed. CA, on the other hand, is also well established as a simple and unique means in the study of nonlinear dynamics, particularly for systems in which the nearest neighbor interaction is predominant [14]. Besides, CA requires only rules (procedures, algorithms) to describe the interaction of neighboring elements, and therefore, one can apply CA to a complicated dynamics that may have no explicit differential and/or integral equations, this situation being frequently encountered in natural and social sciences.

An obvious difference between CA and RD is that RD has a mathematically continuous limit in its solutions, while CA can handle only discrete space-time coordinates. (We are discussing neither the finite difference approximation to differential equations nor the infinitesimal materialization of a space-time unit in CA.) Depending on the size of a system under study, discreteness or the resultant threshold effect on dynamics is naturally installed in CA. Another very important fact to be taken into account is that any symmetry that is inherently involved in a given differential equation cannot be broken within its own scheme without the help of external perturbation, no matter how small it is. This is also the case for the RD. Such an external perturbation (or fluctuation) is quite often applied with the use of artificial noise so as to break the intrinsic determinicity. On the other hand, CA dynamics is naturally driven by a stochastic (probabilistic) procedure. Recently, the importance of fluctuations has been recognized in various phenomena [15–18]. For instance, an

essential difference between macroscopic (having the continuum limit) and microscopic (finite particle systems) dynamics in reaction processes has been ascribed to the fact that even a microscopic fluctuation can be comparable to the main driving forces working on the microscopic composing elements [19,20]. Therefore it is quite interesting to see whether (and how) RD and CA can actually give different results to a same system, provided that a tested system is within their application range.

The paper is organized as follows. In Sec. II, we first introduce the simple growth model mimicking the growth of bacterial colonies, and briefly describe the methodological details of the CA and the standard RD. Further details of the CA are followed by the Appendix. Numerical results directly given by these methods are compared in Sec. III. Section IV is devoted to numerical analyses on how the essential difference between CA and RD has arisen. We actually show that the augmented RD can reproduce the viscous-finger-like complicated pattern. Finally, we conclude this compact paper with some remarks in Sec. V.

II. AUTOCATALYTIC PROLIFERATION OF BACTERIAL CELLS FED WITH NUTRITION AND NATURAL DEATH: MODEL AND METHODS

A. Minimal model mimicking colony formation

We study the growth dynamics of an agent X caused by a simple autocatalytic proliferation and natural death. X proliferates by reacting with another agent N, and naturally dies by the depletion of N (starvation). This model is represented as follows:

$$X + N \rightarrow 2X, \tag{1a}$$

$$X \rightarrow P_1. \tag{1b}$$

Process (1a) A cell (X) takes an amount of nutrition (N), which is prepared with an initial distribution, and proliferates into two pieces by division. Process (1b) A cell (X) dies naturally by starvation with a given rate. The inactive (or dead) bodies (P_1) are left unchanged as they are.

This growth dynamics is designed without respect to biologically inherent and individual mechanisms [21]. Nevertheless, we here call X, N, and P_1, respectively, cell, nutrition, and dead (inactive) body. (In bacterial colony formation, P_1 is actually in the prespore state [13].) In reality, however, these agents can be regarded also as various elements such as chemical reagents and other units of social activity.

B. CA

We next outline the two numerical methods we use in this study, namely, CA and RD. As a means to study the many-particle dynamics of multiple components in general [23], we choose the so-called coupled cellular automata (CCA) [24], in which multiple CA's are connected with each other. Danielak *et al.* developed an extensive CCA in the study of nonlinear interaction between catalytic CO oxidation on the Pt surface and the restructuring of its surface state [25]. We also devised a CCA to represent nonlinear interactions among aggregating particles on a flat surface in the study of cluster formation on a substrate under spatiotemporal fluctuation of temperature [26].

The CCA dynamics applied to the present scheme, Eqs. (1a) and (1b), consists of two CA's (fields): one representing the dynamics of X along with P_1 and the other describing the time-dependent redistribution of N. With these fields, we run the following three procedures (rules): (1) diffusion process on each field (the inactive bodies P_1 do not move, though), (2) reaction process by Eq. (1) through the communication of the two fields for X and N, and (3) the coupling between reactions and diffusion. The last procedure is necessary to handle a situation in which X and/or N happen to have chances of both diffusion and reaction.

The magnitude of diffusion of X represents its mobility, which may also reflect the softness of the substrate, while that of N determines the chance (rate) for X to be fed with. These two diffusion processes on the individual CA fields are regarded as independent stochastic processes, unless they react with each other. The two CA's may be performed on two independent computer nodes and the reaction processes are performed through periodic couplings (communication) between the two fields.

The ratio of time steps of these automata should be determined so as to represent the physical constants predetermined such as those for the reaction rate and diffusions. Otherwise, there is no absolute time unit in the CCA. Each CA field realizes cellular dynamics on two dimensional triangular lattice coordinates, in which any single node has six nearest neighbor nodes, except for those on the boundary. Below we describe the basic CA rules in a rather precise fashion so as to ensure the reproducibility of the present results. We refer to the CCA simply as CA in the following.

1. Diffusion

The particles on each CA field move diffusively, except at the timings of interaction between the two fields for reaction. These diffusive motions are treated as a random walk in each CA field. Each particle is allowed to move to one of its nearest neighbor nodes or remains at the same node. Let p_i be a probability for a particle i to stay at the same node ($0 \leqslant p_i \leqslant 1$). Since particles can diffuse in an isotropic manner, the probability of moving to one of the nearest neighbor nodes is $(1-p_i)/6$ in the present coordinate system. Running a random number in [0, 1), we determine the position to which a particle should move.

2. Reaction

The reaction process is treated as an interaction between the relevant CA fields for X and N. We regard the reaction of Eq. (1a) as a stochastic process and transform the rate constant k as a predetermined probability for particles to react in a unit time.

Furthermore, we introduce two characteristic features of CA rules that are difficult for the ordinary rate theory to describe. The details of the algorithm for the reaction dynamics are given in the Appendix.

3. Coupling of reaction and diffusion

The diffusion processes for X and N on the individual CA's run independently with their own time intervals. They are periodically forced to couple with each other for the reaction in a certain time interval. These timings are fixed by the following relations. Suppose that Δt_{D_i} is a unit time length for the diffusion process of a component i (actually X or N). Also, let Δt_R be the unit time interval for the communication of two CA's to be made to take account of the reaction. Then the relative length for these timings is numerically fixed by predetermining the ratio

$$\tau_i = \frac{\Delta t_R}{\Delta t_{D_i}}. \tag{2}$$

We call this ratio τ_i the diffusion frequency of the component i.

The diffusion frequency τ_i is correlated with the diffusion constant D_i of the component i in the present stochastic model. Choose $|\Delta q|=1$ as a unit length between two nodes of the CA fields, and $\Delta t_R=1$ as a unit time step of the reaction process. Then, the diffusion constant D_i is given in the following form:

$$D_i = \frac{(1-p_i)|\Delta q|^2}{4\Delta t_{D_i}} = \frac{(1-p_i)\tau_i}{4}, \tag{3}$$

where $1-p_i$ is the mobility of particles given above in the description of the diffusion process. Equation (3) suggests that the diffusion constant is proportional to $(1-p_i)$ and τ_i. And thus the diffusion constant of each component can be specified by explicitly choosing p_i and τ_i. (In the coupled cellular automata, the diffusion constant is not treated as a predetermined constant in contrast to the ordinary diffusion equations. See Ref. [26] for a general discussion on the dynamical treatment of the diffusion constants.)

C. RD

We next describe the RD, which naively represent the rate process of the model equations (1a) and (1b) and the diffusion as well. They are

$$\frac{\partial x}{\partial t} = k_1 xn - k_2 x + D_X \nabla^2 x, \tag{4a}$$

$$\frac{\partial n}{\partial t} = -k_1 xn + D_N \nabla^2 n, \tag{4b}$$

$$\frac{\partial p_1}{\partial t} = k_2 x, \tag{4c}$$

where $x(\mathbf{z},t)$, $n(\mathbf{z},t)$, and $p_1(\mathbf{z},t)$ are the spatiotemporal concentration of X, N, and P_1, respectively, in the two-dimensional space $\mathbf{z}$ and time t. k_1 and k_2 are the rate constants of the reaction processes (1a) and (1b), and D_X and D_N are the diffusion constants of X and N, respectively. Since P_1 is inactive and does not move, Eq. (4c) does not include the diffusion term. To integrate these differential equations, we have used the Crank-Nicolson scheme [27] on a grid with a proper mesh size Δz and a time step Δt. In the present paper, we set $k_1=1.0$, $k_2=0.1$, and $D_N=0.25$ throughout. We call Eqs. (4a)–(4c) the standard RD to distinguish our augmented RD to be presented later.

TABLE I. System parameters chosen for the cellular automata.

L	150	Radius of the system
X_0	50	Initial number density of X
p_N	0.33	Probability for N to remain
τ_X	1	Diffusion frequency of X
τ_N	3	Diffusion frequency of N
r_1	0.85	Reaction probability in Eq. (1a)
r_2	0.10	Reaction probability in Eq. (1b)

III. DIFFERENT PATTERNS EMERGING FROM CA AND RD

We apply the above CA and RD to the models (1a) and (1b) to mimic the growth of a bacterial colony. As an initial condition, a tiny circular spotlike colony of X is implanted into a uniform field of N as a seed of its spatiotemporal propagation. The initial concentration of N and the mobility of the individual X are the critical parameters that dominate the dynamics. We have scanned these quantities and other parameters to find the patterns experimentally observed by Matsushita *et al.* [10].

A. Cellular automaton

We first summarize the pattern formation realized by the CA in scanning the two parameters, N_0 (the initial number density of N) and p_X [corresponding to the mobility of X, see Eq. (3)]. Table I lists the system parameters for the present CA. The reflecting boundary condition has been imposed on the CA calculations.

Figure 1 shows the typical growth patterns arising from the four selected values of N_0 and p_X. (Note that the timing to pick the individual patterns is different.) They exhibit the total distribution of X and P_1 without distinguishing them, since the colonies contain both active and inactive (prespore) bacteria and they are not seemingly discriminated from each other. Comparing our numerical results with the experimental morphological diagram [10], we may judge that the present CA has well reproduced the qualitative feature of the colony patterns experimentally observed. On the other hand, our simple calculations were not successful in reproducing the concentric ring patterns observed by Matsushita *et al.* [10,28]. (It is suggested that a particular mechanism that is not contained in our CA rules should work to produce such a concentric colony [29].)

To quantify the complexity of the colony geometry obtained, we calculate the fractal dimension d_f of the patterns by using a relation $S \sim R_g^{d_f}$, where R_g is the radius from the center of mass and S is the area of patterns [see Fig. 2(a)]. As N_0 (p_X) increases (decreases), d_f approaches the space di-

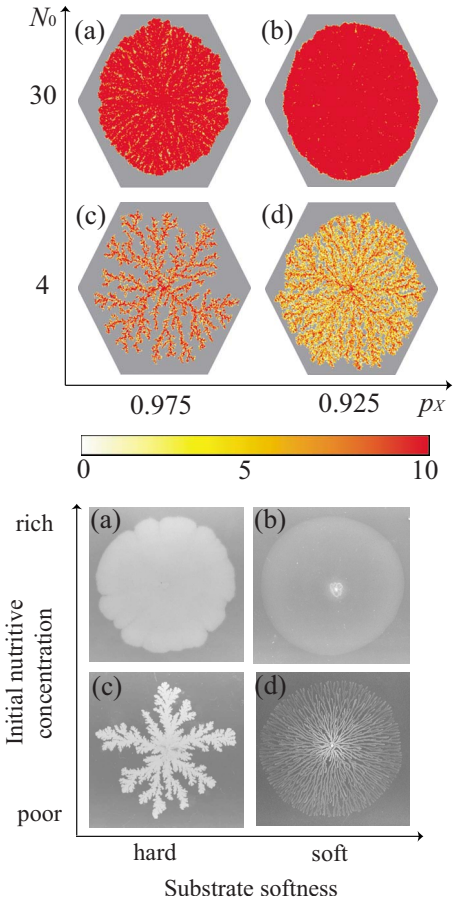

FIG. 1. (Color online) (Upper) Snapshots of the combined distribution of X and P_1 for selected values of N_0 and p_X. Taken at (a) t=730, (b) t=490, (c) t=2830, and (d) t=935. The color bar indicates that the darker (red) part contains the more X and/or P_1 particles. (Lower) Bacterial colonies experimentally observed by Matsushita and his co-workers (reproduced with permission). Incubation time of each colony is about (a) a week, (b) half a day, (c) a month, and (d) a day [28].

mension d=2. In addition, we measure the velocity of growth of the front edge of the colony [Fig. 2(b)]. This figure shows that the front velocity increases as N_0 (p_X) increases (decreases). This result is not surprising and indeed is in harmony with the growth rate of the bacterial colonies experimentally observed [10,28]. It is summarized that in the

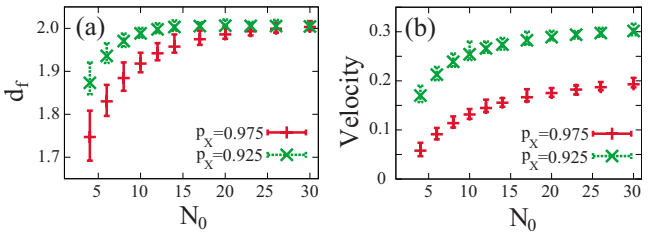

FIG. 2. (Color online) (a) Fractal dimension d_f as a function of N_0 and p_X. d_f approaches the space dimension d=2 as N_0 increases. (b) The front velocity of the propagating colony. The velocity increases, as N_0 increases or p_X decreases. (+) p_X=0.975 (low mobility of X). (×) p_X=0.925 (high mobility).

circumstances where the amount of N is less and X moves slower (less frequent for a larger p_X), the colony grows like a viscous finger with a lower fractal dimension and a smaller growth rate. In such an unfavorable condition, X behaves as though they attempt to elongate their colony boundary in order to make it easier to ingest N. It is quite interesting that such a typical pattern in the diffusion limited aggregation (DLA) [30] can be commonly observed in the systems of nonlinear proliferation. Also, it is rather surprising to see that such an extremely simple mechanical model like Eqs. (1a) and (1b) could reproduce the complicated patterns without respect to the details of biological reality.

B. Reaction-diffusion equations

We next examine the same model as above with the standard RD method. The Neumann boundary condition has been imposed. Again, we have surveyed the possible patterns by scanning the values of two parameters: n_0 (the initial concentration of N) and D_X (the diffusion constant of X).

Interestingly, however, the standard RD method did not generate the complicated growth patterns in marked contrast to the CA. It could generate only a qualitatively circular disk for any values of n_0 and D_X within our examined range (figure not shown). This result suggests that in the mechanical difference between the CA and the standard RD critical factors should exist in the formation of realistic and complicated growth patterns like the viscous-finger-like shape. Thus it is crucial to clarify what is responsible for creating the essential difference between them.

IV. BASIC MECHANISMS GENERATING VISCOUS-FINGER-LIKE ASYMMETRIC BRANCHING PATTERNS

We then analyze the "physical" mechanisms that are responsible for generating the viscous-finger-like fractal pattern in the growth dynamics. Since the CA is already successful in producing such complicated patterns, our analysis is mainly aimed at the properties of the RD equations.

A. Threshold dynamics

As discussed in the Introduction, one of the obvious factors that differentiate the RD equation approach from CA is the treatment of continuity with respect to the variables **z** and t. Mathematically, any small change of the variables is acceptable in the RD equations as an action that may eventually result in a significant effect. Such an assumption (or approximation) of continuity is often unphysical depending on the scale of system size under study. In particular, many physical systems are driven by the so-called threshold dynamics; an event can take place only when a variable excesses a threshold value, with the firing in neural systems being a well-known example. In the present system also, it is not difficult to imagine that the individual cells X can proliferate only after a sufficient amount of nutrition N is consumed. It is therefore natural to begin our analysis with the threshold effect.

To the best of our knowledge, Kessler and Levine are among the first who studied a threshold dynamics in the RD

equation. In their study on a simplest proliferative reaction $A+B\rightarrow 2A$, they assumed that this reaction does not occur if the concentration of A is below a threshold value [19]. However, a clear branching pattern did not emerge in their scheme, although they observed a front instability of the growth patterns (the instability of the front end of the propagating wave). Then, Golding *et al.* briefly reported in their review paper that a branching pattern arose by adding a degradative reaction $A\rightarrow C$ to the Kessler and Levine model [31]. Moreover, they studied the effect of discreteness on various models for patterning in bacterial colonies, and they concluded that the effect of discreteness is small enough to be neglected in their models [32].

On the other hand, Kitsunezaki [33] reported the success of reproducing the viscous-finger-like branching pattern by introducing the nonlinear diffusion term

$$\nabla(D(x)\,\nabla x), \tag{5}$$

with imposing a condition on the density-dependent diffusion coefficient $D(x)$ such that $D(0)=0$ for a hard substrate (agar in which the cells are implanted). This condition is essentially equivalent to introducing a threshold for diffusive motion. In addition, Mimura *et al.* [34] proposed flexible RD equations to reproduce the experimentally observed patterns. In their sophisticated model, the reaction rates are designed to depend on the concentration of x (active bacteria) and n (nutrition). In particular, one of the rates [corresponding to our k_2 in Eq. (4a)] is supposed to be virtually zero if both x and n are larger than threshold values. This also sets a threshold dynamics. Although these pioneering studies are important, it is hard to comprehend what actually happens behind the phenomena observed. We therefore attempt to study further in our own way.

1. Augmentation of the RD equations (1)

To quantify the effect of threshold dynamics, we first define a threshold parameter ε as the concentration of components. With this ε, we define a *quasidiscrete concentration* of X, denoted as x_ε, in such a way that

$$x_\varepsilon \equiv \begin{cases} x & (x \geqslant \varepsilon) \\ 0 & (x < \varepsilon). \end{cases} \tag{6}$$

Similarly, we define n_ε for the component N. With x_ε and n_ε, it is represented that the components whose concentrations are below the threshold are not activated to react. More explicitly, Eqs. (4a)–(4c) are modified as

$$\frac{\partial x}{\partial t} = k_1 x_\varepsilon n_\varepsilon - k_2 x_\varepsilon + D_X \nabla^2 x, \tag{7a}$$

$$\frac{\partial n}{\partial t} = -k_1 x_\varepsilon n_\varepsilon + D_N \nabla^2 n, \tag{7b}$$

$$\frac{\partial p_1}{\partial t} = k_2 x_\varepsilon. \tag{7c}$$

We refer to these as the threshold RD equations. Note that no threshold effect has been taken into account in the diffusion terms. Incidentally, the above modified RD equations are different from those used by Kessler *et al.* [19] and Golding *et al.* [31] in that the threshold effects are consistently considered in all the reaction processes.

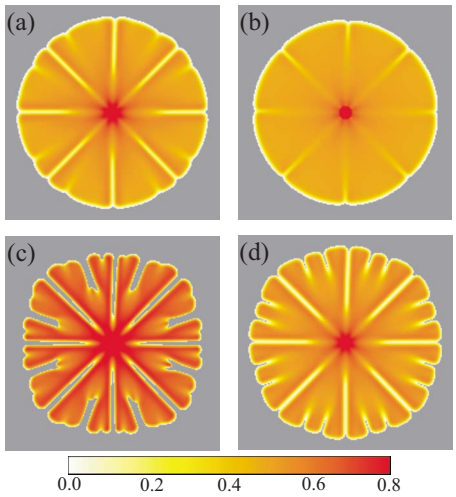

FIG. 3. (Color online) Snapshots of two-dimensional growth patterns (the combined distribution of X and P_1) for selected values of D_X and ε by using Eqs. (7a)–(7c). Taken at (a) $(D_X,\varepsilon)=(0.005,10^{-3})$, $t=2300$, (b) $(D_X,\varepsilon)=(0.010,10^{-3})$, $t=1200$, (c) $(D_X,\varepsilon)=(0.005,10^{-2})$, $t=4500$, and (d) $(D_X,\varepsilon)=(0.010,10^{-2})$, $t=2300$. In these panels, the concentration at each point is depicted as zero if it is below ε. Although clear branching webs appear, the patterns still keep a spatial symmetry.

The patterns emerging from the above threshold RD equations, Eqs. (7a)–(7c), are displayed in Fig. 3. They have been obtained by varying the threshold value ε and the diffusion constant of X. The figures clearly show that the branching patterns have certainly emerged although they are not very akin to the patterns generated from CA (Fig. 1). With this partial success, we next study how the threshold dynamics has brought about the branching shapes.

2. Analysis: Mechanism of the branching induced by threshold dynamics

To extract the essential mechanism that gives birth to the branching patterns, we here study a very simple rectangular system, on the upper edge of which X is distributed uniformly at $t=0$, while N is almost uniformly distributed in the entire space (see Fig. 4.) Again Table II lists the system parameters used but $\Delta z=0.5$. The periodic boundary condition is imposed on the solutions along the vertical axis, while the Neumann boundary condition is imposed along the horizontal axis. We have observed the patterns growing, with varying the threshold parameter ε just as above with the threshold RD equations.

Figure 4 is composed of four sets of the evolution pattern with (a) $\varepsilon=0$, (b) $\varepsilon=10^{-5}$, (c) $\varepsilon=10^{-3}$, and (d) $\varepsilon=10^{-2}$. The left subpanel for each ε shows the distribution of X only, whereas the right counterpart does the joint distribution of X and P_1 as before. It is well observed that as the threshold value ε becomes larger, the clearer branching pattern emerges: When ε is zero [panel (a)] or sufficiently small

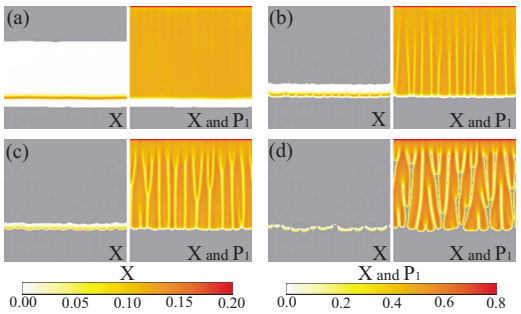

FIG. 4. (Color online) Snapshots of the distributions of X (left) and the sum of X and P_1 (right) for selected ε. (a) $\varepsilon=0.0$, $t=1000$, (b) $\varepsilon=10^{-5}$, $t=1300$, (c) $\varepsilon=10^{-3}$, $t=2100$, and (d) $\varepsilon=10^{-2}$, $t=4700$. When ε is sufficiently large, the wave front of X becomes rough and splits into several small pieces.

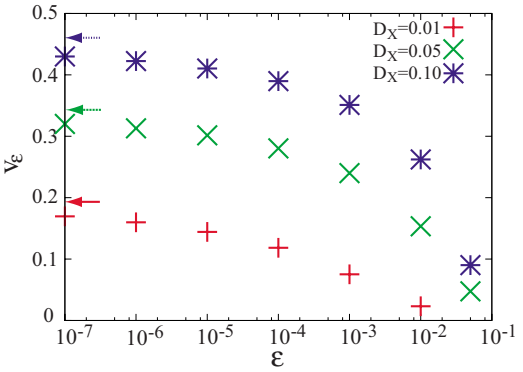

FIG. 5. (Color online) Wave-front velocity v_ε for various ε. The arrows indicate the wave-front velocity at $\varepsilon=0$. As ε becomes larger, v_ε decreases. (+) $D_X=0.01$, (×) $D_X=0.05$, and (*) $D_X=0.10$.

[panel (b)], the wave front of X keeps its shape to be almost flat and thus the growth patterns left behind show almost uniform distributions. On the other hand, the larger ε [panels (c) and (d)] leads the wave front to become rougher, resulting in the clearer branching webs.

These snapshots in Fig. 4 have been taken at different timings; (a) $t=1000$, (b) $t=1300$, (c) $t=2100$, and (d) $t=4700$, indicating that the higher threshold value makes the velocity of the wave front slower. To quantify the relation between the wave-front velocity v_ε and ε, we plot their relations in Fig. 5. (The horizontal arrows in the figure indicate the wave-front velocities of the corresponding D_X at $\varepsilon=0$.) As seen in the graph, v_ε decreases as ε becomes larger, and eventually it is nullified beyond a certain ε. On the other hand, most of the cells X can be found only in the front end of the propagating wave, as the left subpanels of Fig. 4 indicate. New X are produced in the thin region (a beltlike zone) of the wave front, and they eventually change because of the shortage of N, leaving P_1 behind. Thus, the higher threshold ε makes the autocatalytic reaction Eq. (1a) less efficient, and consequently, the resultant slower propagation of the wave front makes the population of X even smaller and the wave front thinner. This fact is clearly observed in the left subpanels of Fig. 4. It is in this situation that disconnection of the belt of the wave front of the cells X takes place here and there. In the areas where the concentration of X becomes lower than the threshold, the proliferation reaction Eq. (1a) stops concomitantly, and after thus broken wave fronts proceed, canal-like zones follow in which both X and P_1 are missing. It is obvious for the same reason that the smaller D_X or the fewer amount of N should assist one in creating the finer branching structure more clearly.

TABLE II. System parameters chosen for the reaction-diffusion equations.

L	200	System size
Δz	0.25	Spatial step
Δt	0.01	Time step
x_0	1.0	Initial concentration of X
n_0	0.5	Initial concentration of N
D_N	0.25	Diffusion constant of N
k_1	1.0	Rate constant in Eq. (1a)
k_2	0.1	Rate constant in Eq. (1b)

The above scenario is compatible with the fact that the sophisticated RD equations previously proposed could reproduce well the branching patterns. To begin with, we note that the threshold in x_ε should reduce the rate for X to be converted to P_1, and should prevent the wave front composed of X from becoming thinner. On the contrary, if the "rate constant" of $X\rightarrow P_1$ is larger for the smaller x, the diminution of the concentration of X in the wave front in the low x region is accelerated and the branching phenomenon should become more prominent. Indeed this mechanism has been explicitly taken into account in the RD equations by Mimura *et al.* [34]. Also, the lowering of the velocity of the wave front can be realized by introducing a threshold into the diffusion of X (recall Fig. 5). This may account for the success of reproducing the branching patterns in terms of the nonlinear diffusion term as introduced by Kitsunezaki [33]. [See Eq. (5) and the discussion below it.]

Thus it turns out that the threshold dynamics is one of mechanisms responsible for producing the branching structures in the proliferation dynamics.

B. Local noise of continuous limit

Another critical difference between the CA and RD lies in the treatment of determinicity; the RD equations, like other well-posed initial value problems, are deterministic and the inherent symmetries incorporated in an initial condition are not broken in the time propagation. (Note that even the propagation of a distribution function for diffusion process is given deterministically.) On the other hand, the individual steps in the CA are usually evolved in time by "tossing dice." Since the threshold dynamics and the stochasticity are physically independent, we study what will result by the stochasticity alone without the effect of threshold dynamics.

To investigate the effect of stochasticity, we introduce "noise" into the standard RD equations (but not threshold) in such a way that

$$\frac{\partial x}{\partial t} = k_1 x n - k_2 x + D_X \nabla^2 x + \eta_1 \xi_1(\mathbf{z},t) - \eta_2 \xi_2(\mathbf{z},t), \quad (8a)$$

$$\frac{\partial n}{\partial t} = -k_1 x n + D_N \nabla^2 n - \eta_1 \xi_1(\mathbf{z},t), \tag{8b}$$

$$\frac{\partial p_1}{\partial t} = k_2 x + \eta_2 \xi_2(\mathbf{z},t), \tag{8c}$$

where $\xi_1(\mathbf{z},t)$ and $\xi_2(\mathbf{z},t)$ are Gaussian noises independently generated at a space-time point $(\mathbf{z},t)$, with η_1 and η_2 being their associated scaling constant, respectively. The system to which we applied these equations is the same as that of the incubation of a spotlike seed. The conditions for this part of the calculations are $n_0=0.5$ and $D_X=0.010$, which are the same as those of the panels (b) and (d) in Fig. 3. The constants to scale the noise are set to $\eta_1=\eta_2=10^{-5}$. The colonies generated by this modification converge to a very simple and clear pattern. It has been observed that X is eventually extinguished almost everywhere, and many small colonies composed mostly of P_1 are left behind (not shown graphically). This conclusion is generic even for the case of small noising parameters η_1 and η_2, and is quite understandable, since the noise in Eq. (8a) results in implanting many seeds of the cells X at many places in a random fashion. Since there is no threshold for them to react with N ($\varepsilon=0$ here), some of them are evolved in time to larger colonies. Then the proliferating cells X eventually consume almost entire nutrition N (recall that X becomes doubled with a single N) and the process ends with $X \rightarrow P_1$. The resultant scattering colonies are of course an artifact.

Thus, it turns out that the introduction of noise should be performed within the context of threshold dynamics, even if they are mathematically independent.

C. Local noise with the threshold: Breaking symmetry

1. Augmentation of the RD equations (2)

We accordingly introduce the noise terms not to the original RD equations but the threshold RD equations, Eqs. (7a)–(7c). They are

$$\frac{\partial x}{\partial t} = k_1 x_\varepsilon n_\varepsilon - k_2 x_\varepsilon + D_X \nabla^2 x + \eta_1 \xi_1(\mathbf{z},t) - \eta_2 \xi_2(\mathbf{z},t), \tag{9a}$$

$$\frac{\partial n}{\partial t} = -k_1 x_\varepsilon n_\varepsilon + D_N \nabla^2 n - \eta_1 \xi_1(\mathbf{z},t), \tag{9b}$$

$$\frac{\partial p_1}{\partial t} = k_2 x_\varepsilon + \eta_2 \xi_2(\mathbf{z},t), \tag{9c}$$

where $\xi_1(\mathbf{z},t)$ and $\xi_2(\mathbf{z},t)$ are again the Gaussian white noises. We refer to these as the locally fluctuating RD equations.

The intensity level of the noises should also be considered so as to be consistent with the threshold dynamics. In a macroscopic description (based on the concentration), $k_1 x_\varepsilon n_\varepsilon$ represents the mean production rate. On the other hand, the mean production rate with a microscopic description (based on the number of particles) should be represented as $c_1 \tilde{x}\tilde{n}$, where c_1 is a probability rate for production, and $\tilde{x}$ and $\tilde{n}$ are the number of particles of X and N in the unit volume Ω. Therefore these two quantities should be correlated with each other in the following relation:

$$k_1 x_\varepsilon n_\varepsilon = \frac{c_1 \tilde{x}\tilde{n}}{\Omega}, \tag{10}$$

and it is estimated as $\tilde{x}=x_\varepsilon \Omega$ and $\tilde{n}=n_\varepsilon \Omega$. Then, the amplitude of the fluctuation can be microscopically estimated at the square root of the mean production rate, $\sqrt{c_1 \tilde{x}\tilde{n}}$, provided that this reaction dynamics is regarded as the Poisson process. Thus the amplitude of the fluctuation with the macroscopic description η_1 is written in as

$$\eta_1 = \frac{\sqrt{c_1 \tilde{x}\tilde{n}}}{\Omega} = \sqrt{\frac{k_1 x_\varepsilon n_\varepsilon}{\Omega}} = \sqrt{k_1 x_\varepsilon n_\varepsilon \varepsilon}, \tag{11}$$

where $\varepsilon=1/\Omega$. In this expression, η_1 includes the threshold value ε explicitly, indicating that the fluctuation becomes larger as the threshold is higher. In a similar manner, we can estimate the amplitude of the fluctuation in the reaction (1b) as

$$\eta_2 = \sqrt{k_2 x_\varepsilon \varepsilon}. \tag{12}$$

Note, however, that this noise expression may become inconsistent with the idea of the Gaussian random process, which generally assumes the presence of a sufficiently large number of particles [35]. On the other hand, as shown above, a large threshold parameter ε tends to reduce the population of X. Nevertheless, we test the locally fluctuating RD equations in what follows.

2. Symmetry breaking induced by the local fluctuation

We recall in Fig. 3 that the threshold for occurrence of the reactions introduced into the RD equations could generate the patterns of branching structures. However, they retain high spatial symmetry, which is not easily broken within its own RD scheme. Obviously, the small fluctuation in the initial distribution of N is not sufficient to break the symmetry significantly, unless the RD solution is unstable and surrounded by symmetry breaking solutions. (Kitsunezaki used a random lattice in numerically solving his RD equations [33].)

Figure 6 shows selected snapshots of the colony pattern resulting from the locally fluctuating RD equations, Eqs. (9a)–(9c), as a function of the threshold value of ε and the diffusion constant D_X. Comparing it with Fig. 3, we immediately notice a large difference: The inner structure of the patterns is now more complicated and far more resembles the colony patterns generated from CA. Thus, the patterns show clear branching webs and the asymmetric morphology.

To quantify the effect of noise on the geometry of resultant colonies, we calculate the fractal dimension d_f [Fig. 7(a)] and the front velocity of the patterns [Fig. 7(b)], varying ε and D_X. d_f approaches the space dimension $d=2$ as ε approaches zero, and the velocity decreases as ε increases or D_X decreases. These figures show almost the same behavior as those of CA. A comparative inspection of Figs. 7 and 2

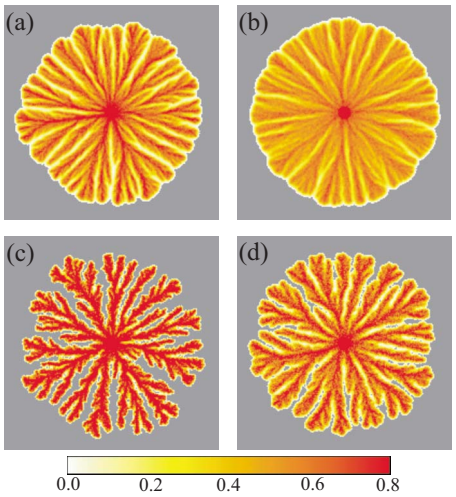

FIG. 6. (Color online) Snapshots of two-dimensional growth patterns (the combined distribution of X and P_1) for different D_X and ε obtained with Eqs. (9a)–(9c). Taken at (a) $(D_X,\varepsilon)=(0.005,10^{-3})$, $t=2100$, (b) $(D_X,\varepsilon)=(0.010,10^{-3})$, $t=1200$, (c) $(D_X,\varepsilon)=(0.005,10^{-2})$, $t=3800$, and (d) $(D_X,\varepsilon)=(0.010,10^{-2})$, $t=2000$. The growth patterns show not only the clear branching structures but also the spatially asymmetric morphology as observed in the patterns generated from CA.

shows that increasing ε in the locally fluctuating RD equations corresponds to decreasing N_0 in the CA method. This can be understood as follows. The presence of a threshold as high as ε practically discretizes the amount of N necessary for the reaction, and therefore N is effectively measured in units of ε. Thus, the higher ε applied to RD as a threshold should make the number count of N smaller for a given initial concentration of N. This is effectively equivalent to reducing N_0 used in the CA.

V. CONCLUDING REMARKS

We have identified the essential origins that make the major differences between the CA and RD, which are also responsible for creating such subtle and complicated structures in proliferation dynamics as the bacterial colony. They are as follows: (i) The threshold effect is necessary for the branching webs to be formed. (ii) Stochastic processes introduced by the internal noise (fluctuation) make the colony patterns asymmetric and decrease the fractal dimension by assisting one in creating more branching webs. In this way, the numerically generated colony attains more realistic forms. Without these factors, the standard RD equations give the colony only a round disk. On the other hand, these physical factors are naturally implemented in the CA. In other words, any system that can be reduced to the type of dynamics of Eqs. (1a) and (1b) with the threshold dynamics and stochastic fluctuation may produce the patterns of Fig. 1.

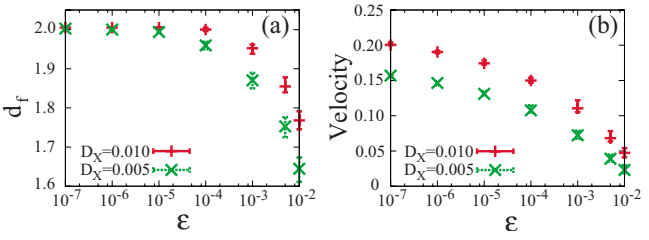

FIG. 7. (Color online) (a) Fractal dimension d_f for selected values of ε and D_X. d_f approaches the space dimension $d=2$ as ε approaches zero. (b) The front velocity of the patterns for different ε and D_X. The velocity decreases, as ε increases or D_X decreases. (+) $D_X=0.010$. (×) $D_X=0.005$.

In the above analyses, we have suggested a systematic method to improve the reaction-diffusion equations so as to include threshold dynamics with local fluctuation. These modifications on the RD extend its application field to a wider range, and would be practically useful in simulating realistic dynamics, in which stochasticity and/or switching (firing) of the onset are crucial.

On the other hand, the roles of stochasticity (vs determinicity) and discreteness (vs continuity) depend strongly on the system sizes under study. For a rather large scale system consisting of many microscopic particles, the system may be well approximated with continuous variables and the deterministic approach should be accurate. Conversely, as the constituent elements like our cells X become larger, and as the discreteness of the elements is apparent, such modifications as we proposed should be vital for the RD approach. For the same reason, a naive application of the CA to a very microscopic and smooth dynamics may lead to unphysical solutions.

We have shown that the comparative study between the CA and RD is quite useful to extract the essential factors dominating pattern formation. Yet, there is a case where neither stochasticity nor discreteness of the variables is the origin of the difference in patterns given by CA and RD. We will report such a dynamics in our future paper [22].

ACKNOWLEDGMENTS

We are grateful to Professor M. Matsushita for providing us with the figures of their studied bacterial colonies. This work was supported in part by the Grant-in-aid for Basic Science from the Ministry of Education, Culture, Sports, Science and Technology of Japan. One of the authors (K.O.) is financially supported by Japan Society for the Promotion of Science for Young Scientists.

APPENDIX: ALGORITHM FOR REACTION PROCESS

Taking X as an example, we here introduce two characteristic features of the CA rules that are difficult for the ordinary rate equation method to describe: Consider the decomposition reaction of X in Eq. (1b). Basically, its rate should depend only on the number of X at each node. However, since X can be involved in the other reaction Eq. (1a) at the same time, the decomposition reaction cannot be treated independently as though no other reactions exist. Thus, the decomposition reaction of X effectively depends on the local circumstances.

In this Appendix, we describe the CA rules in great detail. In what follows, X_i^z denotes the number of X particles at a

node $\mathbf{z}$ before a reaction $\Delta X_+^{\mathbf{z}}$ ($\Delta X_-^{\mathbf{z}}$) indicates the increment (decrement) of X at $\mathbf{z}$ during the reaction, whereas $X_f^{\mathbf{z}}$ does the number of X at $\mathbf{z}$ after the reaction, satisfying $X_f^{\mathbf{z}}=X_i^{\mathbf{z}}+\Delta X_+^{\mathbf{z}}-\Delta X_-^{\mathbf{z}}$. For the other components, the similar notations are used.

1. Treatment of push-out effect

When a single X particle splits into two, one of them can be stochastically pushed out to a neighboring node or remains at the original point. We here define s as a probability for the X particle to stay at the original node ($0 \leqslant s \leqslant 1$). And, since the particle is pushed out to isotropic directions, the probability to be pushed out to one of the nearest neighbor nodes is $\frac{1-s}{6}$. In this paper, we set $s=0.99$ throughout. A random number R in $[0, 1)$ is used to determine a node to which one of two split X particles should move. We denote these nodes as S.

2. CA rules

(1) Perform step 2 to step 4 for all the nodes.
(2) Repeat the next steps $X_i^{\mathbf{z}}$ times at a node $\mathbf{z}$.
(3) Go to the following procedure A:
(A) $X+N \rightarrow 2X$ [Eq. (1a)].
(a) If $N_i^{\mathbf{z}}-\Delta N_-^{\mathbf{z}} \neq 0$, then perform the next substeps (b) and (c). Otherwise, go to step 4 [Eq. (1a) does not occur].
(b) Generate a random number R in $[0,1)$.
(c) If $R<r_1$, then add unity to ΔX_+^S and $\Delta N_-^{\mathbf{z}}$, respectively, and then go back to step 2 [Eq. (1a) occurs]. Otherwise, go to step 4 [Eq. (1a) does not occur].
(4) Go to the following procedure B.
(B) $X \rightarrow P_1$ [Eq. (1b)].
(a) Generate a random number R in $[0,1)$.
(b) If $R<r_2$, then add unity to $\Delta X_-^{\mathbf{z}}$ and $\Delta P_{1_+}^{\mathbf{z}}$, respectively [Eq. (1b) occurs].
(c) Go back to step 2.
(5) After the above procedures are completed, calculate $X_f^{\mathbf{z}}$, $N_f^{\mathbf{z}}$, and $P_{1_f}^{\mathbf{z}}$ for all the nodes.

[1] C. Sachs, M. Hildebrand, S. Völkening, J. Wintterlin, and G. Ertl, Science **293**, 1635 (2001); M. Nagasaka, H. Kondoh, and T. Ohta, J. Chem. Phys. **122**, 204704 (2005).
[2] J. D. Murray, Sci. Am. **258**, 80 (1988); S. Kondo and R. Asai, Nature (London) **376**, 765 (1995).
[3] R. Kapral and K. Showalter, *Chemical Waves and Patterns* (Kluwer, Dordrecht, 1995).
[4] A. M. Turing, Philos. Trans. R. Soc. London, Ser. B **237**, 37 (1952).
[5] A. Gierer and H. Meinhardt, Kybernetik **12**, 30 (1972).
[6] J. E. Pearson, Science **261**, 189 (1993).
[7] K. J. Lee, W. D. McCormick, J. E. Pearson, and H. L. Swinney, Nature (London) **369**, 215 (1994).
[8] Y. Kuramoto, *Chemical Oscillations, Waves, and Turbulence* (Springer-Verlag, Berlin, 1984/ Dover Edition, 2003).
[9] R. J. Field, E. Kőrös, and R. M. Noyes, J. Am. Chem. Soc. **94**, 8649 (1972).
[10] M. Ohgiwari, M. Matsushita, and T. Matsuyama, J. Phys. Soc. Jpn. **61**, 816 (1992).
[11] E. O. Budrene and H. C. Berg, Nature (London) **349**, 630 (1991).
[12] I. Cohen, A. Czirok, and E. Ben-Jacob, Physica A **233**, 678 (1996).
[13] E. Ben-Jacob, I. Cohen, and H. Levine, Adv. Phys. **49**, 395 (2000).
[14] B. Chopard and M. Droz, *Cellular Automata Modeling of Physical Systems* (Cambridge University Press, Cambridge, England, 1998).
[15] T. Shinbrot and F. J. Muzzio, Nature (London) **410**, 251 (2001).
[16] B. Lindner, J. García-Ojalvo, A. Neiman, and L. Schimansky-Geier, Phys. Rep. **392**, 321 (2004).
[17] J. García-Ojalvo and J. M. Sancho, *Noise in Spatially Extended Systems* (Springer, New York, 1999).
[18] C. B. Muratov, E. Vanden-Eijnden, and E. Weinan, Proc. Natl. Acad. Sci. U.S.A. **104**, 702 (2007).
[19] D. A. Kessler and H. Levine, Nature (London) **394**, 556 (1998).
[20] Y. Togashi and K. Kaneko, Phys. Rev. E **70**, 020901(R) (2004); Y. Togashi and K. Kaneko, Physica D **205**, 87 (2005).
[21] This simple proliferation model has been considered as the simplest member of a set of dynamical systems that is of roughly hierarchical structure. Adding new factors (functioning) one by one, we examine what kind of phenomena may appear in a hierarchical manner in thus enlarged systems. By doing so, we attempt to identify the essential factors that can lead to the complexity in pattern formation processes. We have constructed the other two dynamical models; one model system contains an inhibition (repression) process, and the other is enriched with an activation process. The main aim is to comprehend how the pattern formations emerge in an "axiomatic" manner of system construction. Indeed, a series of thus constructed models is found to generate many interesting patterns, which will be reported elsewhere [22].
[22] K. Odagiri and K. Takatsuka (unpublished).
[23] Actually, the CA method used in this paper is similar to a multiparticle model [14], which lies in between the strict CA (or the lattice gas automata) and the lattice Boltzmann method. Nonetheless, we call our used method a CA, because we want to emphasize an advantage of the CA that can handle what is not necessarily reduced to differential equations.
[24] L. G. Morelli and D. H. Zanette, Phys. Rev. E **58**, R8 (1998); P. Grassberger, *ibid.* **59**, R2520 (1999).
[25] R. Danielak, A. Perera, M. Moreau, M. Frankowicz, and R. Kapral, Physica A **229**, 428 (1996).
[26] S. Yaguma, K. Odagiri, and K. Takatsuka, Physica D **197**, 34 (2004).
[27] W. H. Press, S. A. Teukolsky, W. T. Vetterling, and B. P. Flannery, *Numerical Recipes in C*$^{++}$, 2nd ed. (Cambridge University Press, Cambridge, England, 2002).

[28] J. Wakita, H. Shimada, H. Itoh, T. Matsuyama, and M. Matsushita, J. Phys. Soc. Jpn. **70**, 911 (2001).
[29] M. Matsushita (private communication).
[30] T. A. Witten and L. M. Sander, Phys. Rev. Lett. **47**, 1400 (1981).
[31] I. Golding, Y. Kozlovsky, I. Cohen, and E. Ben-Jacob, Physica A **260**, 510 (1998).
[32] I. Cohen, I. Golding, Y. Kozlovsky, and E. Ben-Jacob, Fractals **7**, 235 (1999); E. Ben-Jacob and H. Levine, J. R. Soc., Interface **3**, 197 (2006).
[33] S. Kitsunezaki, J. Phys. Soc. Jpn. **66**, 1544 (1997).
[34] M. Mimura, H. Sakaguchi, and M. Matsushita, Physica A **282**, 283 (2000).
[35] D. T. Gillespie, J. Chem. Phys. **113**, 297 (2000).